

---


Electronic Theses and Dissertations, 2004-2019

---

2013

## Transient Multi-scale Computational Fluid Dynamics (cfd) Model For Thrombus Tracking In An Assit Device Vascular Bed

Ruben Osorio  
*University of Central Florida*

 Part of the [Mechanical Engineering Commons](#)  
Find similar works at: <https://stars.library.ucf.edu/etd>  
University of Central Florida Libraries <http://library.ucf.edu>

This Masters Thesis (Open Access) is brought to you for free and open access by STARS. It has been accepted for inclusion in Electronic Theses and Dissertations, 2004-2019 by an authorized administrator of STARS. For more information, please contact [STARS@ucf.edu](mailto:STARS@ucf.edu).

---

### STARS Citation

Osorio, Ruben, "Transient Multi-scale Computational Fluid Dynamics (cfd) Model For Thrombus Tracking In An Assit Device Vascular Bed" (2013). *Electronic Theses and Dissertations, 2004-2019*. 2673.  
<https://stars.library.ucf.edu/etd/2673>

TRANSIENT MULTI-SCALE COMPUTATIONAL FLUID DYNAMICS (CFD) MODEL FOR THROMBUS  
TRACKING IN AN ASSIST DEVICE VASCULAR BED

by

RUBEN DARIO OSORIO  
B.S. University of Central Florida, 2011

A thesis submitted in partial fulfillment of the requirements  
for the degree of Master of Science  
in the Department of Mechanical, Materials, and Aerospace Engineering  
in the College of Engineering and Computer Sciences  
at the University of Central Florida  
Orlando, Florida

Summer Term  
2013

© 2013 Ruben Dario Osorio

## **ABSTRACT**

Heart failure occurs when the heart is not capable to pump blood at a sufficient rate to meet the demands of the body. Depending on the health of the heart, doctors may recommend a heart transplant, but finding a suitable donor is often a long duration process and the patient might be at an advance condition or the patient is not adequate for a heart transplant. In such cases Ventricular assist devices (VAD) are implemented. The purpose of a VAD is to aid the heart to pump the correct amount of blood, by doing so it relieves the load that is put on the heart while giving the patient a chance for recovery. This study focuses on observing the hemodynamic effects of implementing a left ventricular assist device (LVAD) along the aortic arch and main arteries. Thrombi creation and transportation is other subject included in the study, due to the fact that thrombi can obstruct blood flow to critical arteries, manly carotid and vertebral. Occlusion of these can lead to a stroke with devastating effects on the neurocognitive functions and even death.

A multi-scale CFD analysis a patient specific geometry model is used as well as a lumped system which provides the correct conditions in order to simulate the whole cardiovascular system. The main goal of the study is to understand the difference in flow behavior created by the unsteady pulsatile boundary conditions. The model described in this work has a total cardiac output of 7.0 Liters/ minute, this for a healthy heart. Two cardiac output splits are used to simulate heart failure conditions. The first split consists of 5 Liters/minute flowing through the LVAD cannula and 2 Liters/minute via the aortic root. The second scenario is when heart

failure is critical, meaning that zero flow is being output by the left ventricle, thus a split of 7 Liter/minute through the LVAD cannula and 0 Liters/minute traveling through the aortic root. A statistical analysis for the thrombi motion throughout the patient aortic arch was performed in order to quantify the influence that pulsatile flow has on the particles being tracked. Spherical particles of 2mm, 4mm and 5mm were released and accounted in the statistical analysis for each of the two split configurations. The study focuses on particles that escaped on the outlet boundaries of the upper arteries (Right Carotid, Left Carotid, and Vertebral). Results exhibit the statistical comparison of means for each particle diameter as well as for the overall probability for the steady and unsteady flow condition.

*There is nothing impossible to him who will try*

- Megas Alexandros

## **ACKNOWLEDGMENTS**

I would like to thank God and my Father and Mother for all the support and help given to me though out this adventure, to my brother to inspire me to be the best I can be. Special thanks to Dr. Alain Kassab and Dr. Eduardo Divo for mentoring me and helping me achieve my goals.

## TABLE OF CONTENT

LIST OF FIGURES.....	ix
LIST OF TABLES.....	xi
CHAPTER ONE: INTRODUCTION.....	1
CHAPTER TWO: LITERARY REVIEW .....	4
CHAPTER THREE: THEORETICAL BACKGROUND .....	7
Computational Fluid Dynamics.....	7
Cardiovascular System.....	10
Fluid Dynamics Electrical Analogy .....	14
CHAPTER FOUR: MATERIAL AND METHODS.....	17
One Dimensional Cardiovascular Model .....	17
Computational Fluid Dynamics Model.....	22
Finite Volume Mesh.....	22
Boundary Conditions.....	24
Discrete Element Method – Particle Tracking Model.....	25
Model Coupling between 1D & 3D Models .....	28
CHAPTER FIVE: RESULTS AND CONCLUSION.....	29
One Dimensional Output Results.....	29



Embolism Probability Results.....	37
APPENDIX: ONE DIMENSIONAL CIRCUIT SCHEMATIC.....	43
LIST OF REFERENCES .....	45

## LIST OF FIGURES

Figure 1. Left Ventricular Assistance Device Set Up & Components. What Is a Ventricular Assist Device? Digital image. - NHLBI, NIH. N.p., n.d. Web. 13 May 2013 .....	2
Figure 2 Cardiovascular System of a human. Rich oxygen blood is represented by the red color while low oxygen blood is in blue.....	12
Figure 3. RCL Box, Components used to accurately represent the behavior of each section of the cardiovascular system.....	15
Figure 4 Greenfield-Fry Analogy. Electrical components simulate fluid dynamics behavior in the one dimensional cardiovascular system.....	16
Figure 5 Blood flow path as it travels throughout the cardiovascular system & LVAD.....	18
Figure 6 Atrium & Ventricle representation for the one dimensional cardiovascular model.....	19
Figure 7 Coronary Arterial & Venous Bed, a variable resistor is place in the arterial bed in order to simulate the out of phase flow condition of the coronaries.....	20
Figure 8 Module 4 CFD/ Section of Interest. RL Box is placed between nodes.....	21
Figure 9 CFD Fluid Domain Mesh. 544095 Cells .....	22
Figure 10 Aortic Root mesh detail. Cells become smaller as they approach the wall. ....	23
Figure 11 Mesh near the LVAD Insertion Region, slower cell growth near bifurcation regions. .	23
Figure 12 Location and type of time Dependent Boundary Condition used in the 3D model ....	25
Figure 13 Injection Plane. Grid of 10X5 points from where to sample particles .....	26
Figure 14 Injection plane location with respect to the full fluid domain .....	27
Figure 15 Flow Diagram of Coupling scheme used to pass information between models .....	28

Figure 16 Left Heart Pressures.....	30
Figure 17 Right Heart Pressures.....	30
Figure 18 Cardiac Output waveform measured at the aortic root.....	31
Figure 19 Cardiac Output waveform measured from at the pulmonary root.....	32
Figure 20 LVAD volumetric flow rate waveform at cannula insertion plane .....	33
Figure 21 Left Heart Pressures for the 5-2 LVAD to Cardiac Output .....	34
Figure 22 Right Heart Pressures for the 5-2 LVAD to Cardiac Output.....	34
Figure 23 LVAD Flow for the 5-2 split model .....	35
Figure 24 Left Heart Pressures for the 7-0 LVAD to Cardiac Output .....	36
Figure 25 Right Heart Pressures for the 7-0 LVAD to Cardiac Output.....	36
Figure 26 LVAD Flow for the 7-0 split model .....	37
Figure 27 2mm motion distal to the LSA and descending aorta bifurcation for the 5-0 Model ..	39
Figure 28 2mm motion distal to the LSA and descending aorta bifurcation for the 7-0 Model ..	40
Figure 29 Tracks progression in time while in the fluid domain for 5mm.....	41

## LIST OF TABLES

Table 1. Divergence of the flux of some physical quantities. ....	9
Table 2. Volume percentage in each component of the cardiovascular system (Ottesen et al, 2004) .....	10
Table 3 Embolism Probability in Carotid, Vertebral and Coronary Arteries.....	38

## CHAPTER ONE: INTRODUCTION

Modern society has adopted a less active and unhealthy lifestyle. This can be seen by the increasing dependability on technology in order to complete our daily tasks, such as locomotion, recreation, food (collection and preparation), etc. According to a study made by the World Health Organization (WHO) approximately 17 million people worldwide who die due to cardiovascular diseases every year, on which heart attacks and strokes have the most occurrences (World Health Organization, 2001). Heart Failure happens when the heart loss its normal capability to relax (fill) and contract (eject), thus pumping less blood through the cardiovascular system (Carol Lfavel & Lynne Warner Stevenson, 2001). Treatment involves medication such as Digoxin, can be administered in order to slow down a fast beating heart and increase the force of contraction. Medication is also administered for related conditions, such as coronary artery disease, clot formation, irregular heart rhythms to name a few (Carol Lfavel & Lynne Warner Stevenson, 2001). Patients with advance but not yet critical heart failure can be candidates for implementation of a left ventricular assistance device (LVAD). A Left Ventricular Assistance Device (LVAD) is an axial flow pump, designed to increase the pumping action of a heart that is too sick to function effectively on its own. The purpose of an LVAD in specific is to aid the left ventricle heart (ejecting chamber) to pump the correct amount of blood (6 – 8 Liters per minute) to the systemic segment of the cardiovascular system. LVADs can also be used as a recovery tool as demonstrated by the case study *Left ventricular assist device as a bridge to recovery in a young woman admitted with peripartum cardiomyopathy*

(Oosterom, 2008) The idea is that by reducing the effort made by the failing heart, this can regain its strength and function more close to normal standards.

A typical LVAD is made out of seven components (size can vary depending on the application) inflow tube, pump unit, outflow tube (cannula), power source, driveline and an external controller. Inflow and outflow tubes as well as pump unit are internal components. Figure 1 illustrates a typical LVAD set up with both internal and external components.

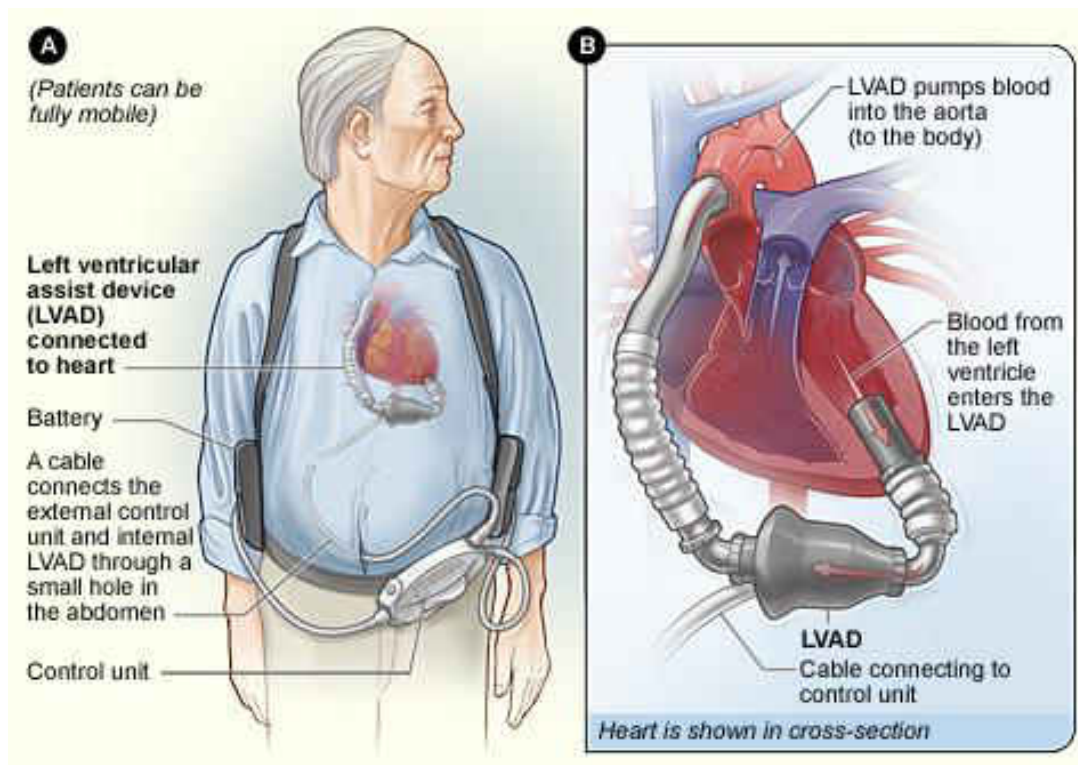


Figure 1. Left Ventricular Assistance Device Set Up & Components. What Is a Ventricular Assist Device? Digital image. - NHLBI, NIH. N.p., n.d. Web. 13 May 2013

Implementation requires performing an incision through the bottom left myocardial muscle in order to access the left ventricle cavity. Once the orifice is made the inflow tube is attached and sutured to the myocardial. Surgeon then attaches the outflow tube to an orifice created proximal to the innominate artery and aortic arch bifurcation. Controller and battery pack are external components that are connected to the pump using a cable. LVADs provide enormous benefits for patients, but it also comes at a cost. Bleeding and clots formation are the most common issues in patients who depend on LVADs. The high shear stress produced by the axial pump, increases the risk of bleeding and arteriovenous malformations (AVMs) in the gastrointestinal (GI) tract (Suarez, 2011). Clot formation is another issue related to axial flow devices. Clots form as side effect of aortic arch bleeding/injury and as well as placket build up inside the internal components of the pump. The risk of stroke is between 10% and 15% per year (World Health Organization, 2001).

The goal of this study is to understand the behavior of blood and how clots interact with the geometry as they travel downstream, and compare the degree of influence that pulsating flow has on clots in hopes of developing a procedure to reduce the risk of a fatal stroke. Apart from a pulsating flow, a human adult aortic arch geometry would be used in order to represent more accurately the actual cardiovascular system.

## CHAPTER TWO: LITERARY REVIEW

Medical Research has played a very important role on extending life expectancy and quality of life of almost all humans from the past century. Vaccines, medical treatments/procedures, drugs, devices have been made available to the public after an extensive research and development. LVAD devices fall into this group of developments as well, but there still a lot of unknowns related to the effects on behavior of the cardiovascular system as well as the adaptation of the human body with a foreign device. As mention before LVADs aid to improve the life of certain persons, but at the same time it also introduces risks to their lives. Understanding how LVADs affect the hemodynamic behavior in the cardiovascular system will allow for a better contingency and control procedures to manage these risks better. This study attempts to closely mimic all conditions that influence the hemodynamic behavior within the aortic arch and main arteries, while utilizing an adult aortic arch as geometry. The novelty of this work is that combines most of the topics of previous individual studies, such as unsteady three dimensional flow in the human aortic arch (N. Shahcheraghi, 2002), Effect of LVAD outflow conduit insertion angle on flow through the native aorta (K.D. May-Newman, 2004), etc. Particle release and tracking particles is an important future of this investigation and for the research of LVADs devices since it will allow for testing hypothesis relating cloth formation and locomotion in a pulsating flow as well as full integration of a lumped parameter one dimensional model with the CFD simulation.



The work described in this document is a follow up to an early study “Computational Fluid Dynamics Analysis of Surgical Adjustment of Left Ventricular Assist Device Implantation to Minimize Stroke Risk” by (Osorio AF, 2013). This early study was carried on by personnel of the cardiovascular e... research team (CERT) at the University of Central Florida. The study analyzed the hemodynamic behavior within the aortic arch, and it also traced particles that were released from the inflow lvad conduit in direction towards the aortic arch. A synthetic computer aid model (CAD model) was used as geometry for this study. Even though the CAD model dimensions are accurate to medical data, it does not fully account for the twist and irregularities found on a human aorta. Boundary conditions for the CFD simulation were not time dependent, a constant flow of 3 L/min and 1 L/min trough the Aorta plane and LVAD plane were imposed, respectively. Outlet conditions were imposed as flow split percentages, not enabling to capture the change in flow that occurs when dealing with a pulsating flow. Spherical particles with diameter ranging from 2mm to 5mm were releases and tracked as they progressed downstream. Statistical analysis was made in order to obtain the probability of particles been displaced towards vital arteries.

Osorio et al (2008) concluded that the location and angle of insertion of the inflow LVAD cannula does affect the blood behavior as well as particle (cloths) locomotion within the aortic arch. Bypass implementation also aids to promote a better flow patter, thus reducing the probability of stroke. The results from the study also open the possibility of tailoring an optimal configuration for each patient with aims of reducing stroke chances of LVAD patients.

Unsteady flow conditions have been prescribed to early studies, providing the ability to model the cardiovascular system more accurately. A CFD study by (N. Shahcheraghi, 2002) aim was to demonstrate the flow (blood) behavior inside the aortic arch undergoing a pulsating motion. An inlet condition at the Aortic root was set to be a flat wave profile plus a pulsatile waveform obtained from previous experiments, while outlet conditions were set to be flow split (flow percentage) leaving for each corresponding branch. Percentage values were obtained from Middleman [36]. The geometry model used for the simulation was reconstructed from a 2D CAT scan from a young patient. A numerical algorithm used to approximate the solution of the equations governing the fluid motion was developed by the research group. A system of motion equations were based on a second order finite volume approach. Preconditioned versions of GMRES were incorporated in order to reduce the computational effort required to attain a converged solution.

Results found by (N. Shahcheraghi, 2002) describe the presence of two flow behaviors within the model; the first flow (main aorta segment) had a tendency of been skewed towards the inner aortic wall, while the secondary flow pattern (aorta branches) was skewed far face with some traces of reverse flow along the proximal wall. Shear stresses were also identified to be higher along the distal wall when compared to the proximal wall. Other important finding was the formation of an M-shaped velocity profile, this probably produced by the curvature in the aortic arch and the presence of the arterial branches. N. Shahcheragi et al (2002) also mention that the flow does not bring to mind the classical steady flow in pipes solution, but it tended to be skewed towards the outer aortic wall

## CHAPTER THREE: THEORETICAL BACKGROUND

### Computational Fluid Dynamics

Computational Fluid Dynamics (CFD) utilizes finite element methods (FEM) and finite difference method (FDM) with the purpose of solving the various differential equations that correctly model fluid behavior. FDM has dominated CFD solution schemes, thanks to its simplicity and faster computational time, in the other hand FEM show the opposite trend. Thanks to advancements in computer technology, this has allowed for more complex problems, while increasing the resolution of the solutions and reducing computing time thus allowing users to have a choice of method (Chung, 2002). FDM and FEM differ in the form of how the differential equations are solved. The first one utilizes small (finite) difference equations to approximate the solution of the general differential equation, while FEM uses variational calculations to reduce the error in the solution of the boundary value problem. Independent of method the solution should be stable and unique.

Starccm+ a commercial CFD code was used to complete this study due to convenience and ease of meshing and post-processing capabilities. Details of CFD simulation set up and schemes used on the study are specified on later sections. Three groups of equations are used to describe flow undergoing deformation; Continuity, Momentum and Energy. Equations 1-5 present these equations in their respective group.

Continuity equations

$$\frac{\partial \rho}{\partial t} + \nabla \cdot (\rho \vec{V}) = 0 \quad (1)$$

Momentum equations

$$x - \text{component} : \frac{\partial(\rho u)}{\partial t} + \nabla \cdot (\rho u \vec{V}) = -\frac{\partial p}{\partial x} + \frac{\partial \tau_{xx}}{\partial x} + \frac{\partial \tau_{yx}}{\partial y} + \frac{\partial \tau_{zx}}{\partial z} + \rho f_x \quad (2)$$

$$y - \text{component} : \frac{\partial(\rho v)}{\partial t} + \nabla \cdot (\rho v \vec{V}) = -\frac{\partial p}{\partial y} + \frac{\partial \tau_{xy}}{\partial x} + \frac{\partial \tau_{yy}}{\partial y} + \frac{\partial \tau_{zy}}{\partial z} + \rho f_y \quad (3)$$

$$z - \text{component} : \frac{\partial(\rho w)}{\partial t} + \nabla \cdot (\rho w \vec{V}) = -\frac{\partial p}{\partial z} + \frac{\partial \tau_{xz}}{\partial x} + \frac{\partial \tau_{yz}}{\partial y} + \frac{\partial \tau_{zz}}{\partial z} + \rho f_z \quad (4)$$

Energy equation

$$\begin{aligned} \frac{\partial}{\partial t} \left[ \rho \left( e + \frac{v^2}{2} \right) \right] + \nabla \cdot \left[ \rho \left( e + \frac{v^2}{2} \vec{V} \right) \right] = \\ \rho q + \frac{\partial}{\partial x} \left( k \frac{\partial T}{\partial x} \right) + \frac{\partial}{\partial y} \left( k \frac{\partial T}{\partial y} \right) + \frac{\partial}{\partial z} \left( k \frac{\partial T}{\partial z} \right) - \frac{\partial(up)}{\partial x} - \frac{\partial(vp)}{\partial y} - \frac{\partial(wp)}{\partial z} \\ + \frac{\partial(u\tau_{xx})}{\partial x} + \frac{\partial(v\tau_{yx})}{\partial y} + \frac{\partial(w\tau_{zx})}{\partial z} + \frac{\partial(v\tau_{xy})}{\partial x} + \frac{\partial(w\tau_{yz})}{\partial y} + \frac{\partial(u\tau_{zy})}{\partial z} \\ + \frac{\partial(w\tau_{xz})}{\partial x} + \frac{\partial(u\tau_{xy})}{\partial y} + \frac{\partial(v\tau_{yz})}{\partial z} + \rho \vec{f} \cdot \vec{V} \end{aligned} \quad (5)$$

These equations apply for a fluid crossing a control volume that was fixed in space. Fluxes (mass/momentum/energy) become the dependent variables in these equations. Inspecting the previous equations, one can see that all equations on their left hand side contain a divergence term, which in terms is the flux of the dependent variables. For an unsteady problem, these terms can be grouped in a vector U, which will take on been the solution vector because the elements in U ( $\rho$ ,  $\rho u$ ,  $\rho v$ , etc.) are the dependent variables which are usually solved numerically

in steps of time. Primitive variables can then be obtained in a simple calculation (Chung, 2002).

Table 1 summarizes the physical meaning and mathematical form of each of these fluxes.

*Table 1. Divergence of the flux of some physical quantities.*

$\rho \vec{V}$	Mass Flux
$\rho u \vec{V}$	Flux of x-component of momentum
$\rho v \vec{V}$	Flux of y-component of momentum
$\rho w \vec{V}$	Flux of z-component of momentum
$\rho e \vec{V}$	Flux of internal energy
$\rho \left( e + \frac{V^2}{2} \right) * \vec{V}$	Flux of total energy

By inspecting the conservation form of each of the equations (1-5) we can rearrange them in to a common form Equation 6. This form is used to represent the complete model of governing equations in the conservation form.

$$J = \frac{\partial U}{\partial t} + \frac{\partial F}{\partial x} + \frac{\partial G}{\partial y} + \frac{\partial H}{\partial z} \quad (6)$$

Equation 6 is composed of flux terms (F,G,H) one source term (J), vector U is the solution vector on which the dependent variables are solved using numerical techniques (Chung, 2002).

## Cardiovascular System

The cardiovascular system is one of the major organ systems with in the human body. Its function is to transport oxygen, nutrients and other supplies required by muscles and organs to carry out a proper function (Ceballos, 2011) . An adult human has an average volume of blood of about 5 Liters (Taggart, 2008).Blood is mainly plasma, about 55% and the other 45% is cellular material such as, leukocytes and platelets, white and red blood cells. Cardiac output ranges from 6 to 8 liters per minute. The system itself can be split into two circulations, the systemic (high pressure sub-system) and the pulmonary circulation (low pressure sub-system). Due to the different operating pressures blood volume is also distributed throughout the system. Volume distribution for each major component is shown in Table 2.

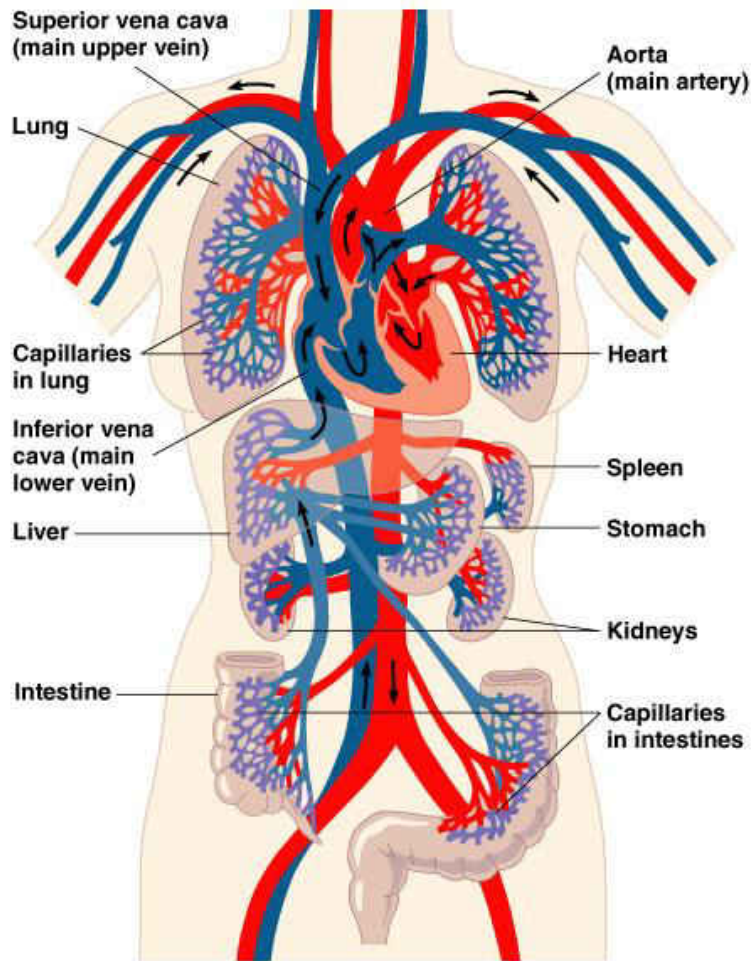
*Table 2. Volume percentage in each component of the cardiovascular system (Ottesen et al, 2004)*

Component	Volume
Arteries	20%
Veins	54%
Lungs	14%

The heart acts as the link between the two circulations as well as the pump that drives the complete system. Four compartments make up the main structure of the heart, left and right atrium, left and right ventricle. The interventricular septum separates the two ventricles and it also provides aid in the pumping action of the left heart. A total of four valves control the blood

flow pattern and timing inside the heart. The mitral valve is located between the left atrium and the left ventricle thus controlling the filling action of the ventricle, on the right side the tricuspid valve performs this task. Outflow valves located at the pulmonary and aortic root prevent blood to flow out the heart while the filling process is occurring. Once the ventricles are filled and the ventricles begin to collapse, pressure increases thus creating a pressure difference between each ventricle and each circulation system making the valves open and allow blood to flow to the respective systems.

Once oxygen rich blood is pumped by the left ventricle of the heart and then travels through the arteries (systemic circulation), providing all the supplies needed for normal cellular function of the different organs, during this process the blood receives most of the waste products that were generated by the cells, mainly carbon dioxide. The low oxygenated blood travels along the veins (systemic circulation) until it returns to the heart via the inferior and superior vena cava. Low oxygen content blood makes its way to through the right heart to then being rushed out to the lungs (pulmonary circulation) where carbon dioxide is exchanged for oxygen, thus enriching the blood with oxygen once again. Pulmonary veins return the re-oxygenated blood to the heart filling the left heart and starting the process once again. . Figure 2 displays the cardiovascular system, with all main components.



Copyright © 2004 Pearson Education, Inc., publishing as Benjamin Cummings.

*Figure 2 Cardiovascular System of a human. Rich oxygen blood is represented by the red color while low oxygen blood is in blue*

The two circulations exhibit different behaviors and properties. As previously mentioned the systemic circulation is known for been the high pressure system while the pulmonary circulation is the low one. The difference in the two behaviors is due to the different length and number of organs that each supply, for example the systemic circulation encounters more resistance due to all the organs needed to be supplied, while the pulmonary circulation only deals with the lungs. Systemic Vascular Resistance (SVR) is the sum of all the resistance created



by the peripheral vasculature within the systemic circulation. It can be computed using Equation 7. Normal values for SVR yield pressures of 120 mmHg in systole and 80 mmHg in diastole.

$$SVR = 80 * \frac{\text{mean arterial pressure} - \text{mean right atrial pressure}}{\text{Cardiac Output}} \quad (7)$$

Pulmonary Vascular Resistance (PVR) is the standard manner of measuring the resistance of the pulmonary circulation. It stands for the resistance that the flow needs to overcome in order to push the blood through the pulmonary circulation. PVR is approximately 1/10<sup>th</sup> of the SVR. Average pressure values for a human adult is 34 mmHg in systole and 13 when in diastole. Equation 8 shows the mathematical form of how to calculate the pulmonary vascular resistance.

$$PVR = 80 * \frac{\text{mean pulmonary arterial pressure} - \text{mean pulmonary artery wedge pressure}}{\text{Cardiac Output}} \quad (8)$$

Both systemic and pulmonary resistances can be combined to obtain the total cardiovascular resistance. Arteries and veins are compliant therefore they do not affect the resistance values in a significant manner.

I

### **Fluid Dynamics Electrical Analogy**

Analysis of the behavior and complexity of the cardiovascular system it's a field in which many studies have been performed. Independent of what the area of study is the first and mandatory step is to accurately represent the behavior of the complete cardiovascular system. The Greenfield-Fry's electrical analogy states that it is possible to simulate the fluid viscous drag as a resistor, flow inertia with an inductor and compliance of the vessel with a capacitor element (Ceballos, 2011). The first one dimensional or lumped parameter was constructed with one resistor and one capacitor in a parallel configuration; it is called Windkessel proposed by Otto Frank. Modified models have been developed in order to give more resolution to the obtained solution (B. Deswysen, 1980). In this study we implemented a modified Windkessel model with one resistor, one capacitor and one inductor as components (RCL Box) Figure 3. The systemic and pulmonary circulations were divided into sections and for each section a RCL box was placed. Refer to Appendix: One Dimensional Circuit Schematic for the complete one dimensional cardiovascular system schematic. All the RCL boxes are connected thus creating a close loop system when joined by the left and right heart models.

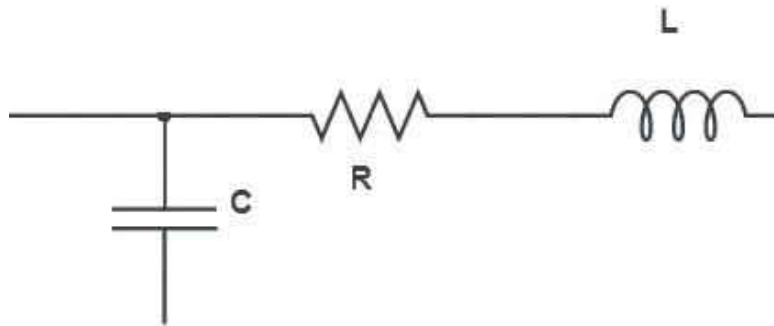


Figure 3. RCL Box, Components used to accurately represent the behavior of each section of the cardiovascular system.

The equations used to model each component are essentially the same form as the electrical equivalent; the only difference is the labeling of the principal parameters. In order to understand why this is possible we must look into the differential form of the Navier-Stokes equations in cylindrical coordinates, Equation 9.

$$\frac{1}{r} * \frac{\partial(r \frac{\partial u}{\partial r})}{\partial r} = \frac{1}{v} \frac{du}{dt} + \frac{1}{\mu} \frac{dP}{dx} \quad (9)$$

Assumptions such as Poiseuille flow, Newtonian fluid are introduced therefore simplifying the differential Navier-Stokes equation (8). After some manipulation the following expressions are obtained;  $C = \frac{dV}{dP}$  (compliance of the vessel),  $Q = \frac{dV}{dt}$  (Volumetric Flow rate). It can be seen from these two expressions that  $Q$  can be related to  $C$  by solving for  $dV$  in  $Q$  and then substituting this expression in  $C$ , resulting in Equation 10.

$$Q = \frac{dV}{dt} = C \frac{dP}{dt} \quad (10)$$

From the previous expressions we can relate the electrical parameters to the fluid dynamic one. Pressure is to electrical potential (Voltage Drop), and volumetric flow rate to current (I) across

an electrical component. Replacing these parameters into the Ohm's law, and equations for current across a capacitor and potential due to the presence of an inductor we can express every component as a pressure or flow rate. Figure 4 summarizes the analogy and presents the general equation for each component.

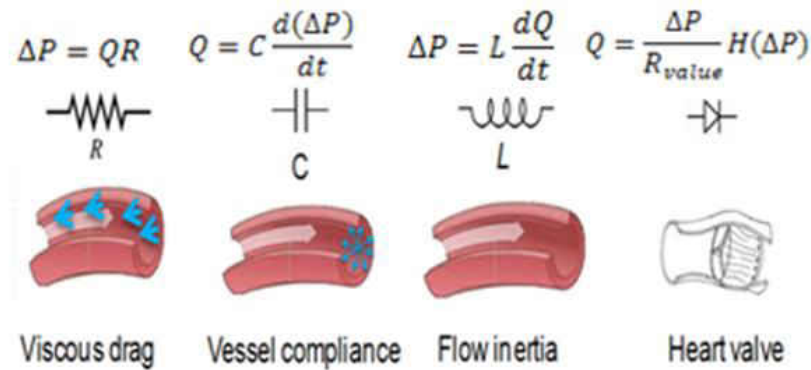


Figure 4 Greenfield-Fry Analogy. Electrical components simulate fluid dynamics behavior in the one dimensional cardiovascular system. (Ceballos, 2011)

Each component of the one dimensional model can be expressed in pressure or flow rate terms. Kirchhoff voltage and current law is performed at every node of the circuit yielding two differential equations per RCL Box, Equation 11 corresponds to the pressure at the given node, Equation 12 relates the volumetric flow leaving the node.

$$\frac{dP}{dt} = \frac{1}{C} (Q_{in} - Q_{out}) \quad (11)$$

$$\frac{dQ}{dt} = \frac{1}{L} (P_{node} - Q_{out} * R - P_{node+1}) \quad (12)$$

## CHAPTER FOUR: MATERIAL AND METHODS

### **One Dimensional Cardiovascular Model**

The purpose of the one dimensional model is to accurately generate the correct boundary conditions. This is achieved by solving the differential equations generated by each RCL Box placed in the complete one dimensional model. The first step in this process is to determine the number of division within each module. In our case we expanded the systemic circulation RCL box so we can include the CFD region, Arterial Vascular Bed & Venous Vascular Bed. The model contains 50 differential equations that are solved simultaneously (Refer to previous chapter for equation derivation).

The system was divided into seven modules in order to simplify the labeling of each node. Module function was the determinant for segmentation. The first module in the system deals with the arterial and venous bed of the lungs, two RCL Boxes one for each bed. Modules 2 and 7 are the right side and left side of the heart, in this order. The LVAD has its own module, 3 due to the special behavior of the device. Module number 4 is the aortic arch and main arteries. Module 5 represents the coronary arterial and venous bed, this due to the fact that coronary flow is out of phase with the main flow. Figure # shows a schematic of blood path throughout the one dimensional model.

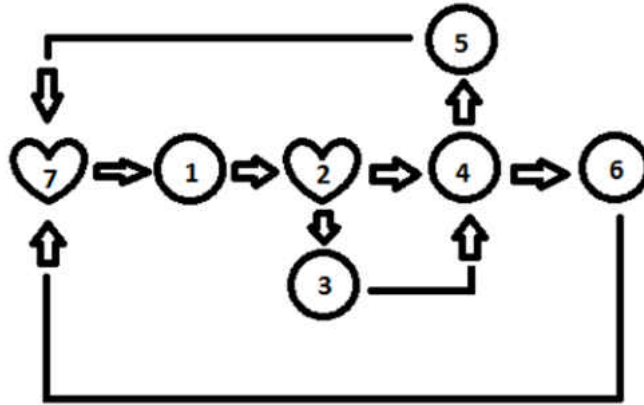


Figure 5 Blood flow path as it travels throughout the cardiovascular system & LVAD

The heart (2 & 7) posed a challenge due to inability of model it as a voltage source (battery) because continuity was not been satisfied due to the creation of current/flow rate. As in a study by (George Faragallah, 2012) we approximate the ventricle behavior by using a time dependent capacitor. The capacitor is modeled by using the inverse of the elastance function of the ventricle. Elastance is the ratio between the ventricle pressure  $VP(t)$  and the ventricle volume  $VV(t) - V_0$  ( $V_0$ –initial ventricle volume at pressure zero), Equation 13.

$$E(t) = \frac{VP(t)}{VV(t)-V_0} \quad (13)$$

As previously mention the heart is divided in two halves, left heart and right heart. Equations used to model ventricles are identical except for labeling of the functions. Equation 14 & 15 are the left ventricle and right ventricle functions.

$$E_{lv}(t) = (E_{max} - E_{min}) * E_{l_n}(t) + E_{min} \quad (14)$$

$$E_{rv}(t) = (E_{max} - E_{min}) * E_{r_n}(t) + E_{min} \quad (15)$$

$R_n$  is the double hill function, which is defined as Equation 16.

$$E(t) = 1.55 * \left[ \frac{\left(\frac{t}{T_{max/0.7}}\right)^{1.9}}{1 + \left(\frac{t}{T_{max/0.7}}\right)^{1.9}} \right] \left[ \frac{1}{1 + \left(\frac{t}{T_{max/1.17}}\right)^{21.9}} \right] \quad (16)$$

Figure 6 is a schematic of the modified RCL Box that is used to model the left and right side of the heart. The valves of the heart are model as diode that has a value of one (open) for the period when the pressure difference between the ventricle and the aortic/ pulmonary root is positive, otherwise the diode has a value of zero (close).

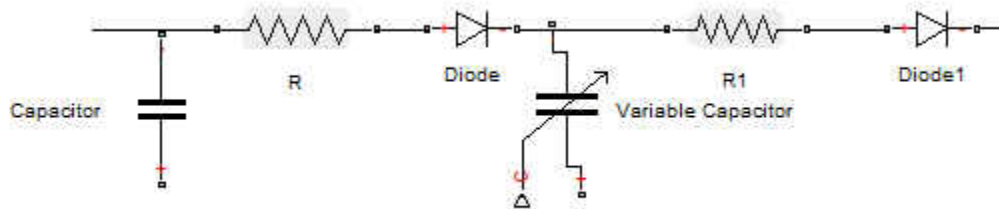


Figure 6 Atrium & Ventricle representation for the one dimensional cardiovascular model.

The coronary bed (5) is other module that requires a special treatment due to the out of phase flow behavior. In order to simulate this phenomenon a variable resistor is implemented in the arterial bed section. The variable resistor takes into count the heart elastance to rise or decrease the resistance value, the mathematical expression used can be seen in Equation 17.

$$R(t) = 1.75 \left[ \frac{E_{lv}(t)}{E_{lv}(0)} \right]^2 + R_{bed} \quad (17)$$

There is no need to model the resistor of the venous bed as variable because it is downstream with respect to the arterial bed therefore experiencing the same fluid motion as the upstream

section. Flow inertia in the coronaries is almost null thus allowing removal of the inductance term in this module. Figure 7 shows the arterial and venous bed of the coronaries.

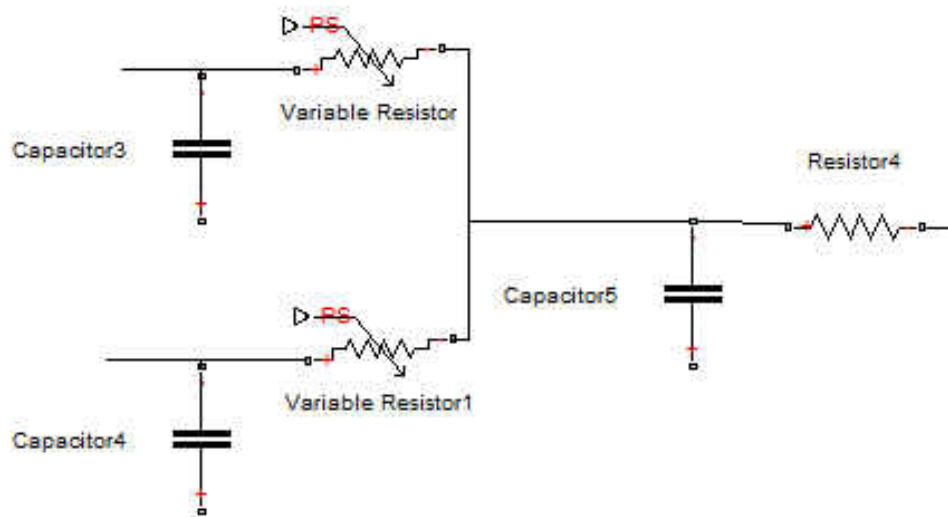


*Figure 7 Coronary Arterial & Venous Bed, a variable resistor is place in the arterial bed in order to simulate the out of phase flow condition of the coronaries.*

Module 4 was divided into 18 RL Boxes, this was done to increase the resolution of the multi-scale model. The capacitor term was omitted since we assumed a non-compliant aortic wall for this study. All RL Boxes can be seen in Figure 8. The resistor and inductor value are updated after each iteration that the multiscale model performs.



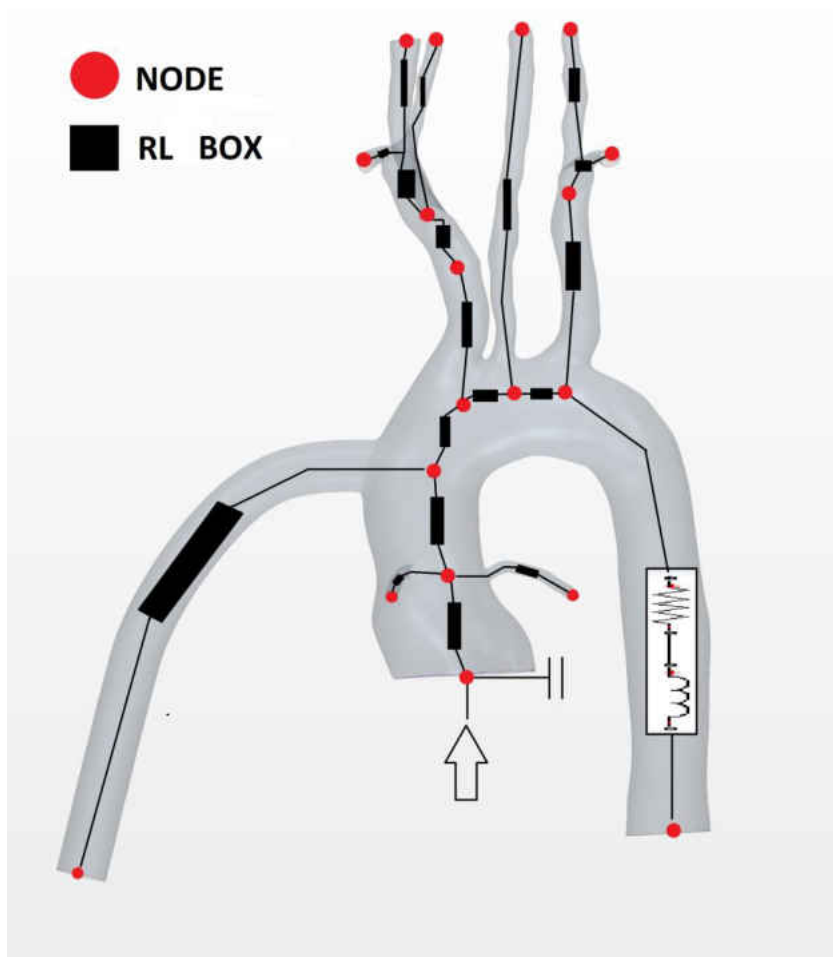


Figure 8 Module 4 CFD/ Section of Interest. RL Box is placed between nodes.

## **Computational Fluid Dynamics Model**

### **Finite Volume Mesh**

The patient specific geometry was meshed using the Starccm+ 8.02. A total of 544095 cells were created for this model. Mesh was refined on the bifurcations to allow a proper capture of the flow behavior near these regions, as well as the incorporation of prism layers near the wall. The obtained model was used for all the particle tracking simulations performed in this study. Figure 9 - 11 show the generated mesh, the mesh near the LVAD cannula insertion, and the aortic root mesh



*Image taken from Starccm+ 8.02 visualization window.*

*Figure 9 CFD Fluid Domain Mesh. 544095 Cells.*

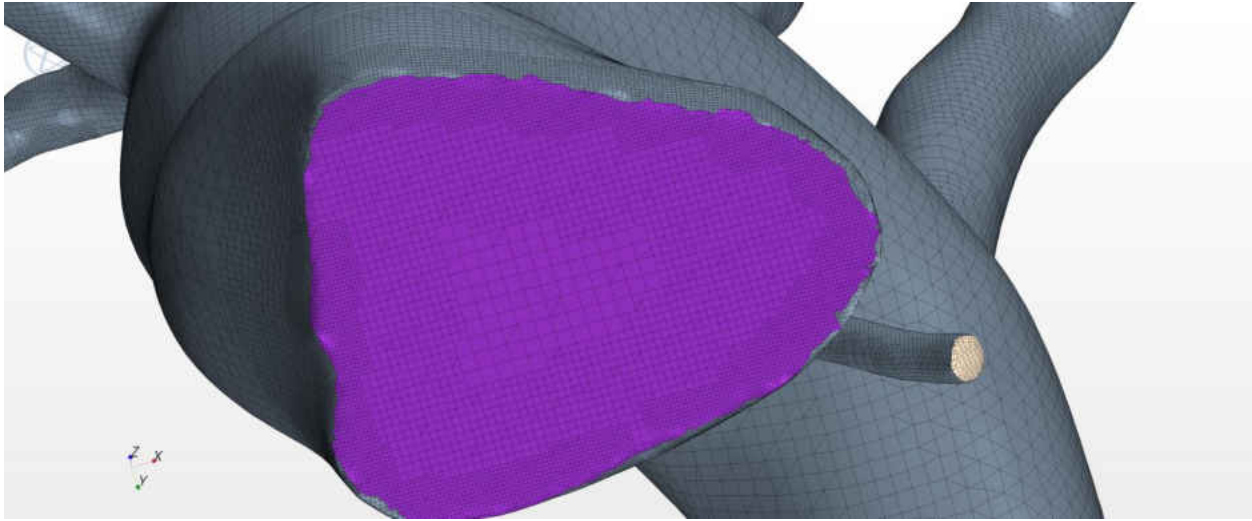


*Image taken from Starccm+ 8.02 visualization window*

*Figure 10 Aortic Root mesh detail. Cells become smaller as they approach the wall.*

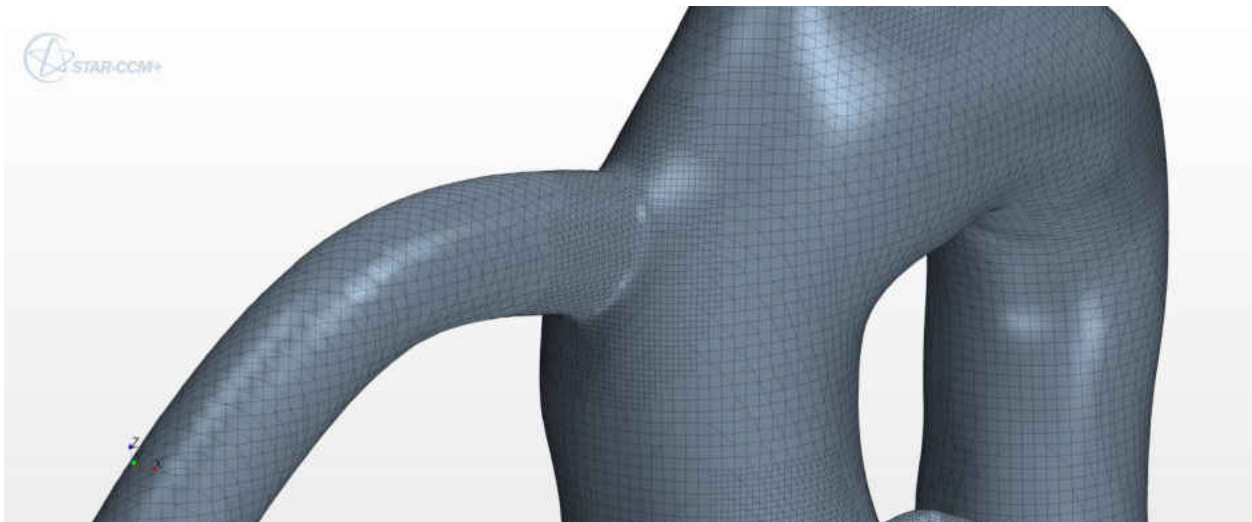


*Image taken from Starccm+ 8.02 visualization window*

*Figure 11 Mesh near the LVAD Insertion Region, slower cell growth near bifurcation regions.*

### **Boundary Conditions**

Boundary conditions are the most important thing when it comes to a CFD problem, and it can be said that the obtained solution is directly product of these conditions. In this study three different types of time dependent boundary conditions were utilized. A mass flow outlet condition was prescribed to all the outlets of the model. Flow been introduce by the LVAD was model by a mass flow inlet condition and finally a stagnation pressure inlet condition was assigned to the Aortic root. The system is driven by the pressure from the aortic root and by the mass being introduce by the LVAD. Figure 12 shows the locations were each boundary condition was imposed.

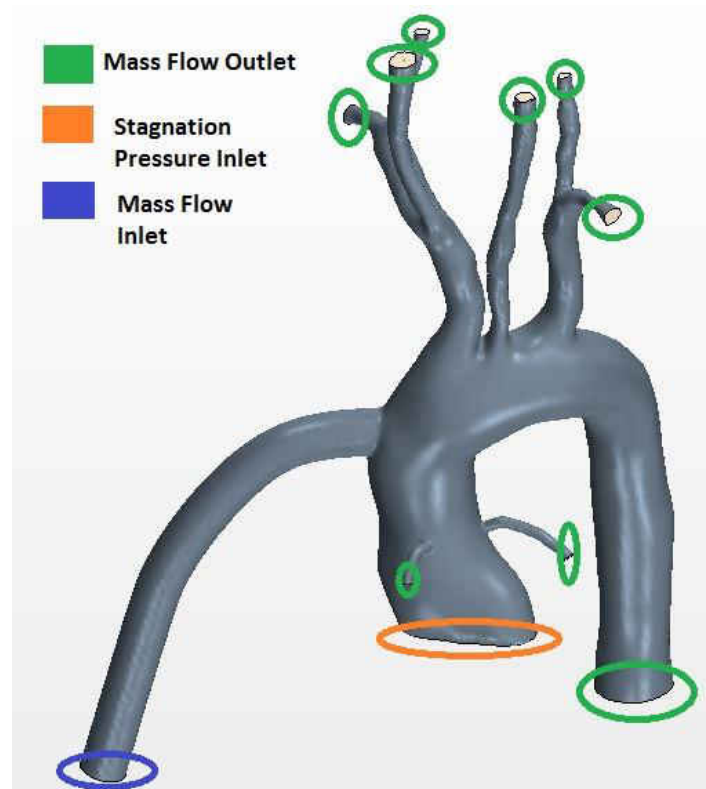


*Figure 12 Location and type of time Dependent Boundary Condition used in the 3D model*

### **Discrete Element Method - Particle Tracking Model**

Spherical particles of 2mm, 4mm and 5mm diameter were released from an injection plane located just above the LVAD cannula region to ensure that the particles were introduced to the fluid domain. The injector plane is represented as a grid of 10 by 5 points, the points that fell outside the fluid domain are not sampled. Figure 13 shows the plane injection grid and its location with respect to the entire model is shown on Figure 14.



*Figure 13 Injection Plane. Grid of 10X5 points from where to sample particles*



*Figure 14 Injection plane location with respect to the full fluid domain*

The Discrete Element Method scheme was turned on, in order to allow particles to interact with each other and with the wall. Collisions for both phase interactions were modeled as perfectly elastic. The Saffman Lift forces as well as the Schiller-Naumann drag model were used to compute for particle body forces. Gravity and Buoyancy force were not included in the study due to the minimal force contribution created by these two forces. Particles are released from 0.0 sec to 1.0 sec, releasing the particles during the time at which the LVAD mass flow is increasing. All the boundaries except the wall are permeable for the particle phase.

### **Model Coupling between 1D & 3D Models**

Coupling between the two models is a process that entitles five steps. The first step deals with the 1D model, from this step we obtain our initial pressure and mass flow wave forms for each boundary condition. These waveforms are then passed as boundary conditions to the CFD solver, not before converting them into the proper units. Pressure was converted from mmgH to Pa, while mass flow was converted from a volumetric flow rate mL/sec to Kg/s. Once the Boundary conditions are accepted by the CFD solver, we ran the simulation. As output from the CFD simulation we acquire pressure and mass flow at different locations within the fluid domain. These scalar values are used to compute the newest resistances and inductances values for the CFD Module (4) The process is perform until the cardiac output was more or less the same. Figure 15 is a flow diagram of the coupling performed between the 1D and 3D models.

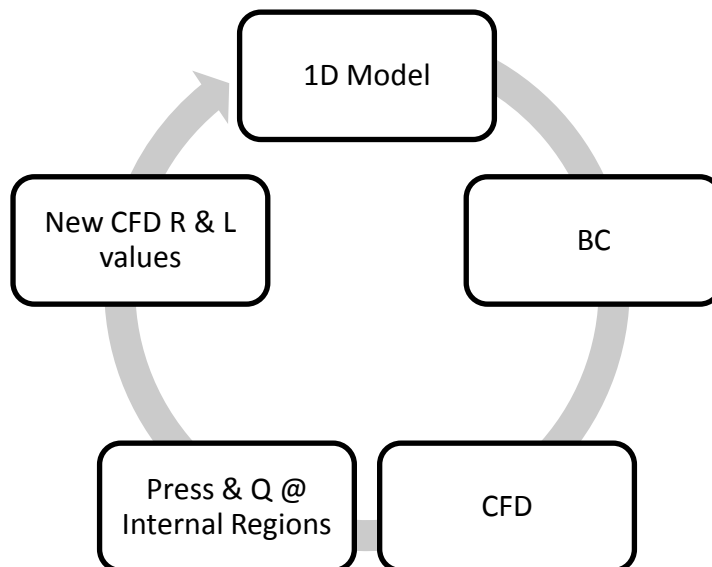


*Figure 15 Flow Diagram of Coupling scheme used to pass information between models*



## CHAPTER FIVE: RESULTS AND CONCLUSION

The main purpose of this study was to find the effect that a pulsatile flow has on the embolism provability on mayor arteries. As expected the thrombi motion is determined by the forces excreted by the fluid that is surrounding it. In the same context it can be stated that the fluid is directly correlated to the boundary conditions imposed in the system, for this special reason the results section is structured by first displaying the results for the one dimensional model and then proceeding to the particle tracking CFD results.

### One Dimensional Output Results

The base line configuration for the analysis was the case for which the LVAD presence was not felt by the rest of the one dimensional circuit. This was achieved by multiplying the LVAD differential equation by zero and setting its initial condition to 0.001 ml/s. The base line model was tuned to achieve the proper pressure and flow, values and waveforms. Figure 16 shows the pressure wave for the load felt by the left ventricle and the aortic root pressure. Values for the aortic root pressure were 126 mmHg in Diastole and 76 mmHg in Systole. Left heart experienced a pulmonary root pressure of 27 mmHg in Diastole and 8 mmHg in Systole, Figure 17. It is important to point out that the ventricular and aortic as well as pulmonary root pressures are in the normal range of an adult person.

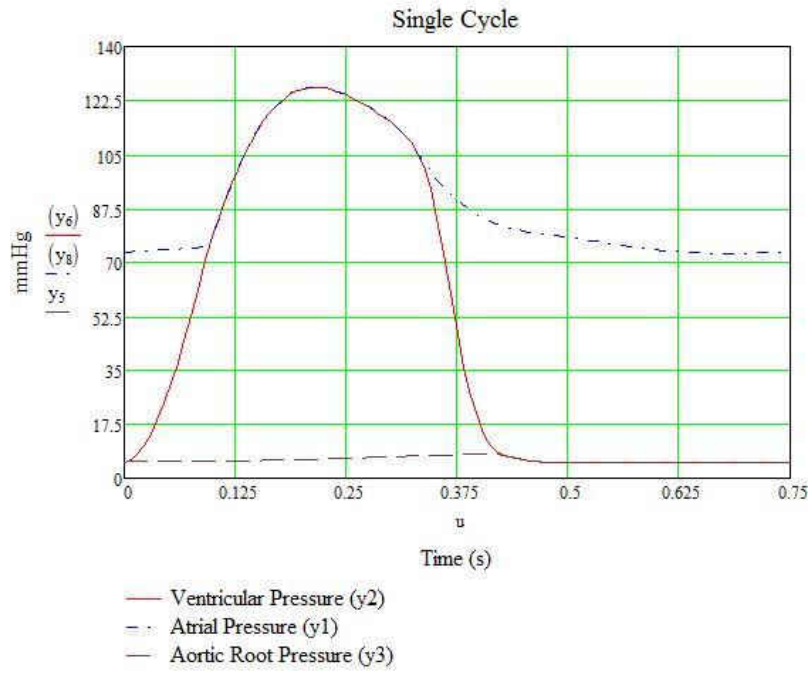


Figure 16 Left Heart Pressures

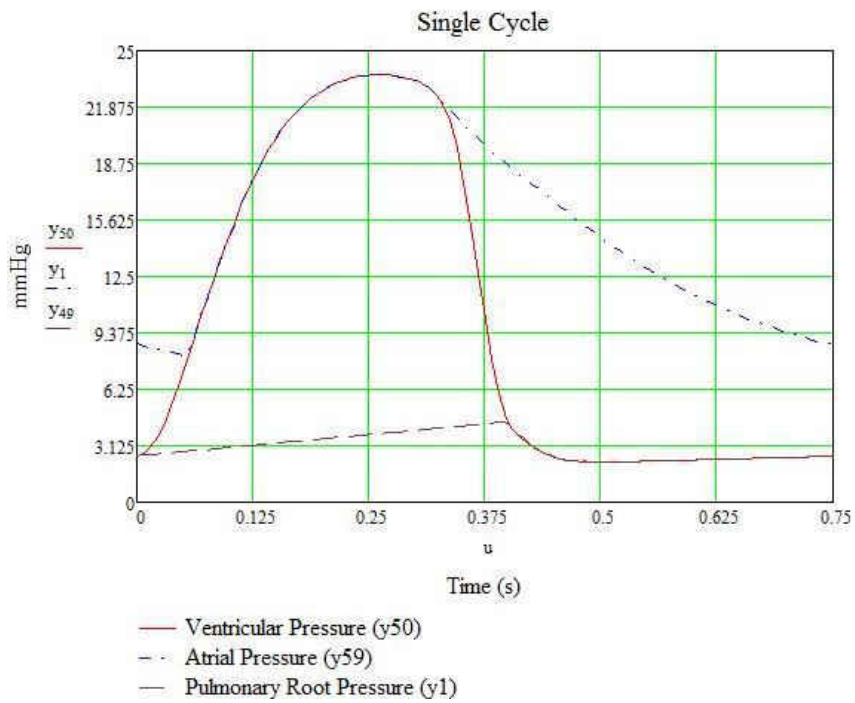


Figure 17 Right Heart Pressures

Other important result obtained from the base line configuration was the cardiac output. Approximately 7.0 Liters per minute are pumped by the heart. The cardiac output can be measured at the aortic root or pulmonary root. In our model both sides of the heart evacuate the same amount of blood. Figure 18 corresponds to the cardiac output waveform measured at the aortic root, while Figure 19 was when measured at the pulmonary root.

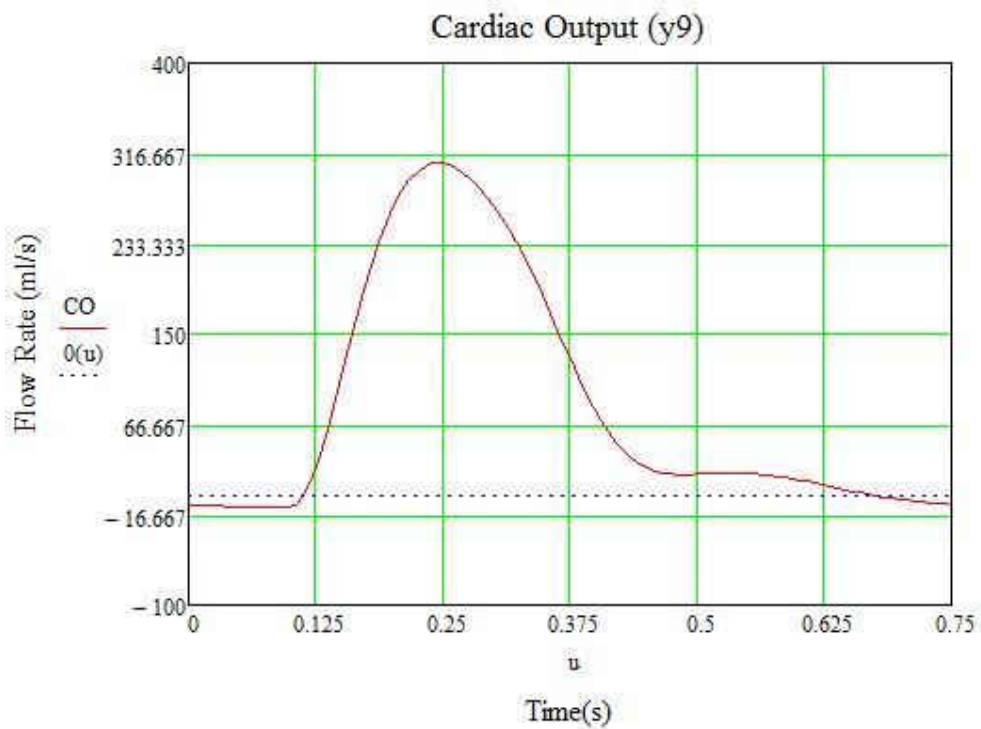
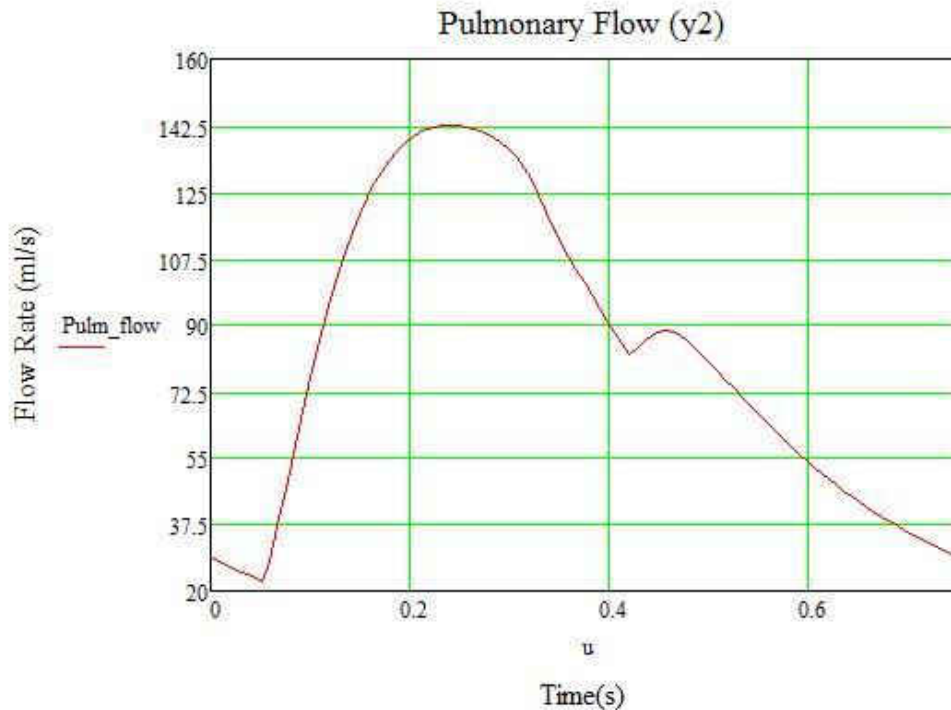


Figure 18 Cardiac Output waveform measured at the aortic root



*Figure 19 Cardiac Output waveform measured from at the pulmonary root*

The different waveforms are due to the different compliance level of each system. Since the systemic circulation compliance is small, the cardiac output wave does not resemble the pressure wave of the aortic root, in the other hand the pulmonary circulation exhibits a large compliance, making its cardiac output wave to closely follow its root pressure (Li, 2004).

Figure 20 confirms that the presence of the LVAD is null, here we can see that the volumetric flow introduced by the LVAD is approx 0.001 ml/sec (its initial condition).

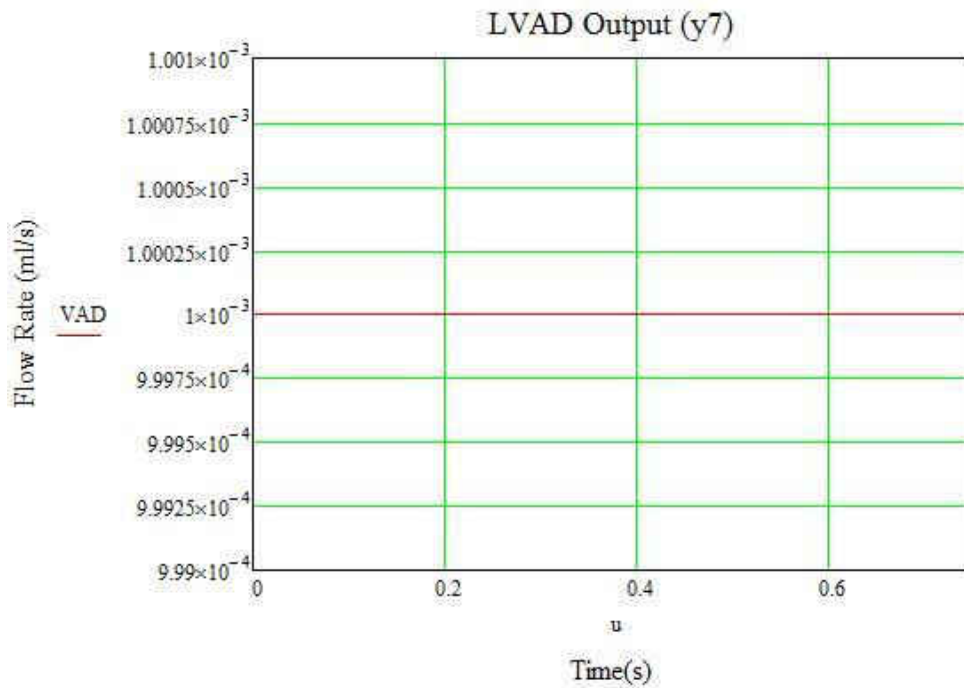


Figure 20 LVAD volumetric flow rate waveform at cannula insertion plane

The base model was then tuned to the two different LVAD to Cardiac Output ratios (5-2 and 7-0 L/min) that were set to analyze. In this set of results we show how the pressure waveforms change due to the LVAD. The strength of the current ( $i_{vad}$ ) supplied to the pump inside the LVAD was either raised or lowered with the goal of attaining the previously mentioned splits. The system does not account for ventricle collapse in the case when the LVAD extracts more blood than what is available inside the ventricle. Figure 21 and Figure 22 display the new pressure waveforms for each side of the heart with a split of 5-2 L/min.

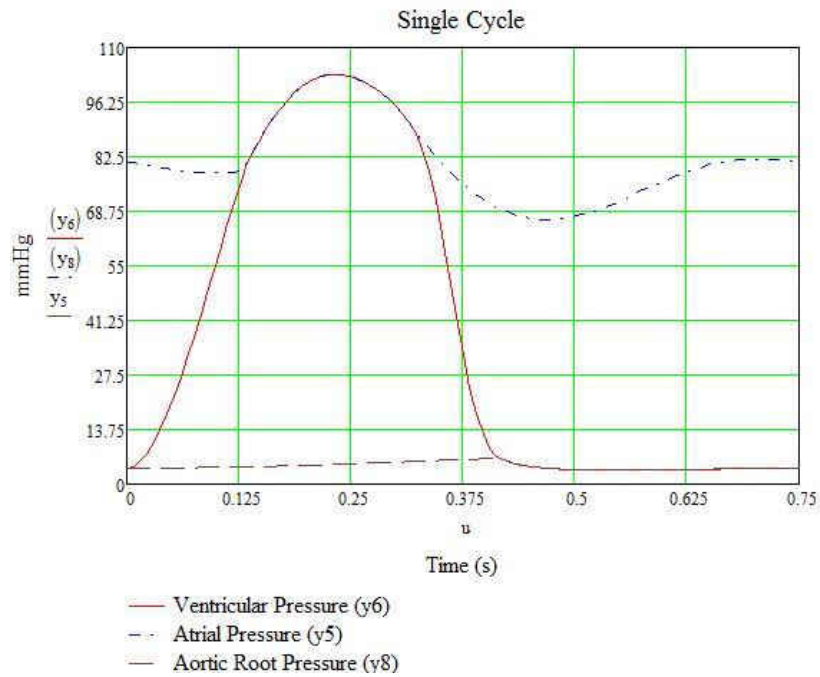


Figure 21 Left Heart Pressures for the 5-2 LVAD to Cardiac Output

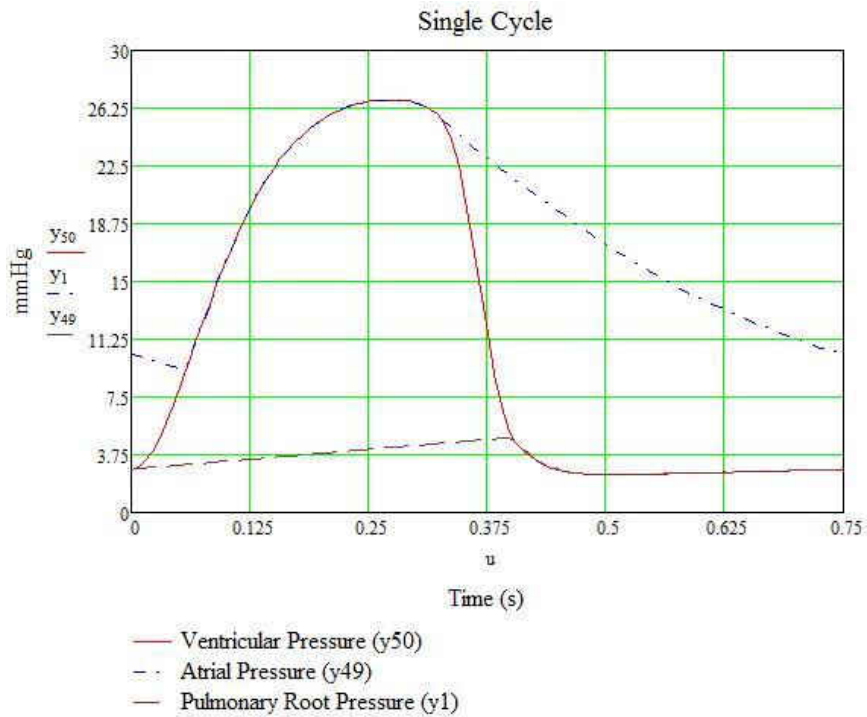
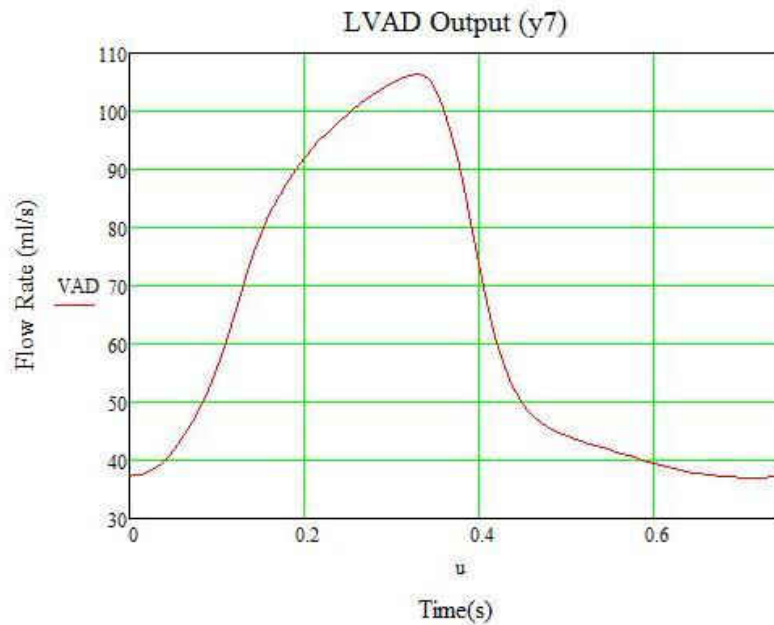


Figure 22 Right Heart Pressures for the 5-2 LVAD to Cardiac Output

The volumetric flow rate introduced by the LVAD does follow the pulsating nature of the ventricle; the main difference is that there is no reverse flow in the cannula. This was expected since the pump is a continuous and its propeller that only allows spinning in one direction. Figure 23 corroborates the fact that the LVAD flow reaches a peak at the same moment in time as the pressure at the ventricle is at its maximum.



*Figure 23 LVAD Flow for the 5-2 split model*

Equal plots are displayed below for the second LVAD to Cardiac output configuration (7-0 L/min). Figure 24 to 26 correspond to Left Heart Pressures for the 7-0 LVAD to Cardiac Output, Right Heart Pressures for the 7-0 LVAD to Cardiac Output and LVAD Flow for the 7-0 split model, in this order.

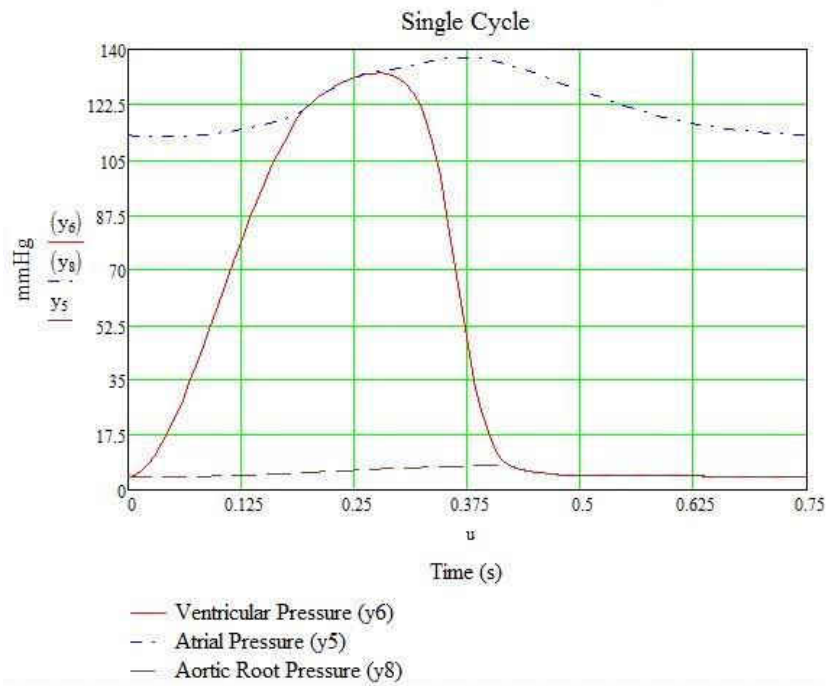


Figure 24 Left Heart Pressures for the 7-0 LVAD to Cardiac Output

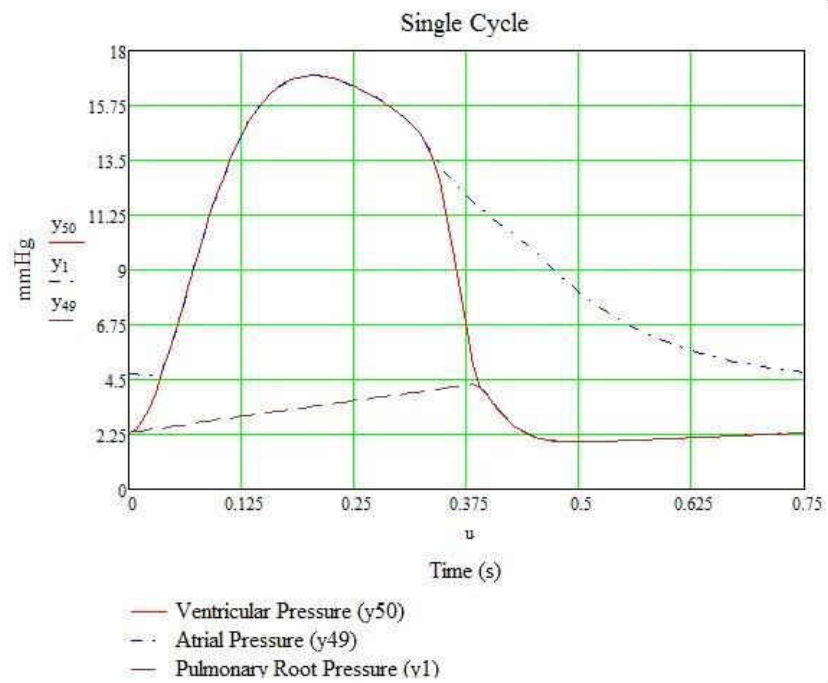
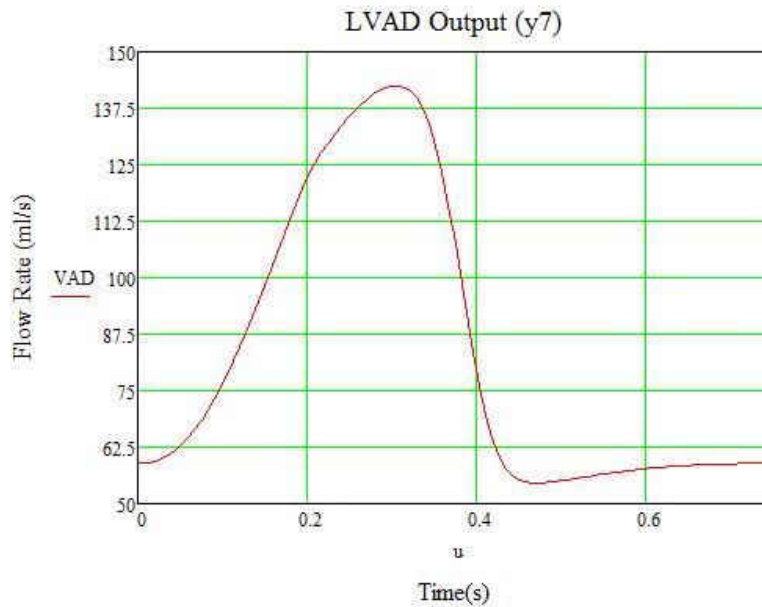


Figure 25 Right Heart Pressures for the 7-0 LVAD to Cardiac Output





*Figure 26 LVAD Flow for the 7-0 split model*

### **Embolism Probability Results**

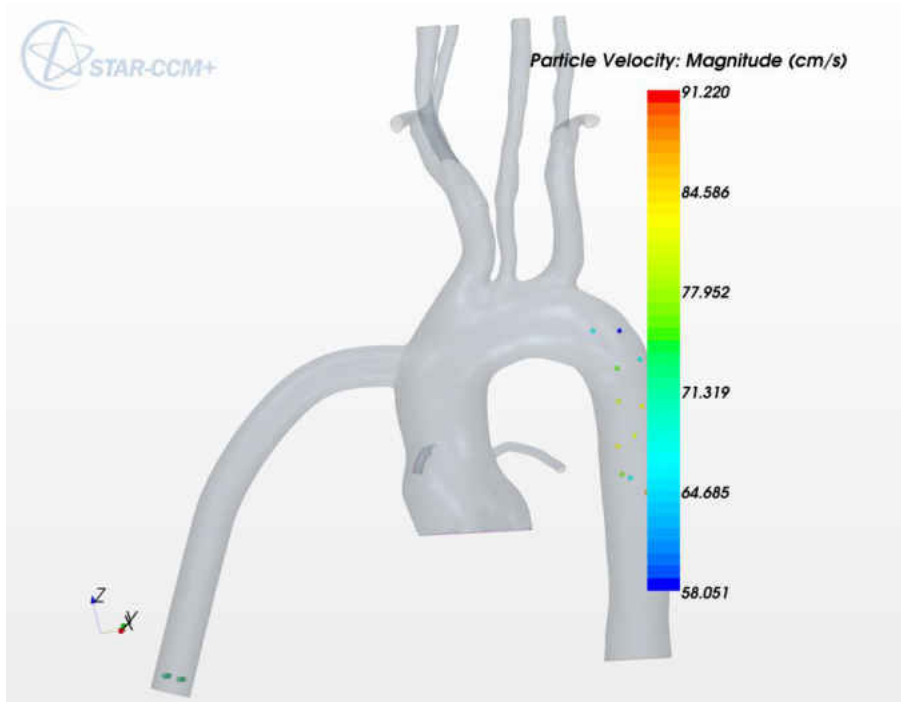
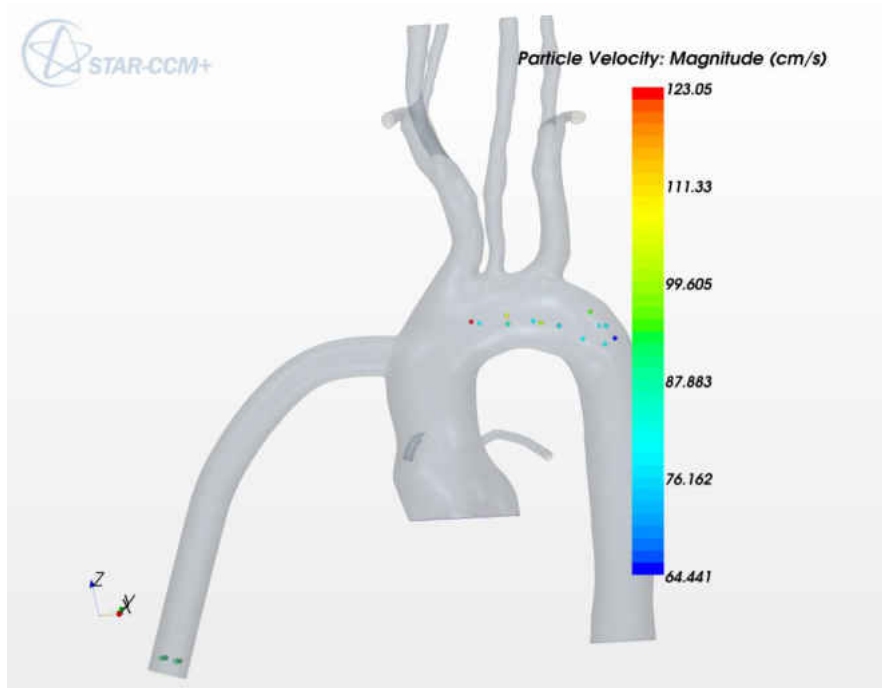
Particles released at the injection plane were tracked through a complete cycle of 0.75 seconds. Fluid domain and particle tracks are solved simultaneously by Starccm+ 8.02; approximate computational time was of 3 hrs for one cycle. Boundary sampling at each outlet region was set up in order to count the number of spherical particles leaving the fluid domain. A mean provability was calculated and compared for both steady and unsteady simulations. A total of two trials were performed for all particles. Due to the particle to particle interaction particles are not allow to over impose each other, therefore reducing the number of sampled particles as its diameter increased. Sample size for the 2mm particles was 127 for 4mm particles sample size was 15 and 11 for 5mm particles.

Table 3 summarizes the particle behavior observed in both steady and unsteady simulations.

*Table 3 Embolism Probability in Carotid, Vertebral and Coronary Arteries*

<b>Configuration</b>	<b>2mm Thrombi [%]</b>	<b>4mm Thrombi [%]</b>	<b>5mm Thrombi [%]</b>	<b>Overall [%]</b>
LVAD_7-0_CO_Steady	4.34	21.73	13.91	13.33
LVAD_7-0_CO_Unsteady	8.62	24.13	5.26	10.36
LVAD_5-2_CO_Steady	10.92	16.8	16.8	14.84
LVAD_5-2_CO_Unsteady	14.17	11.11	4.76	6.04

From the summary table it can be observed that the steady state studies show a small difference in overall probability between the two steady flow cases, while when comparing the unsteady flow probability percentages we notice a reduction of almost four percent when comparing the LVAD\_7-0\_CO\_Unsteady case with the LVAD\_5-2\_CO\_Unsteady. This reduction in probability is directly related to the particle interaction with the aortic wall. Figure 27 shows how the sequence of how the 2mm LVAD\_5-2\_CO\_Unsteady particles interacted with the wall, Figure 28 corresponds to the 2mm LVAD\_7-0\_CO\_Unsteady particles. Due to the higher velocity of the LVAD jet in the 7-0 model particles collide with the aortic arch wall in two locations, thus reducing particle momentum and dispersing the particles towards the main arteries. The slower jet of the 5-2 model provides the particles with enough momentum so they follow the stream that was in the direction of the descending aorta and not impacting with the aortic wall.



*Image taken from Starccm+ 8.02 visualization window*

*Figure 27 2mm motion distal to the LSA and descending aorta bifurcation for the 5-0 Model*

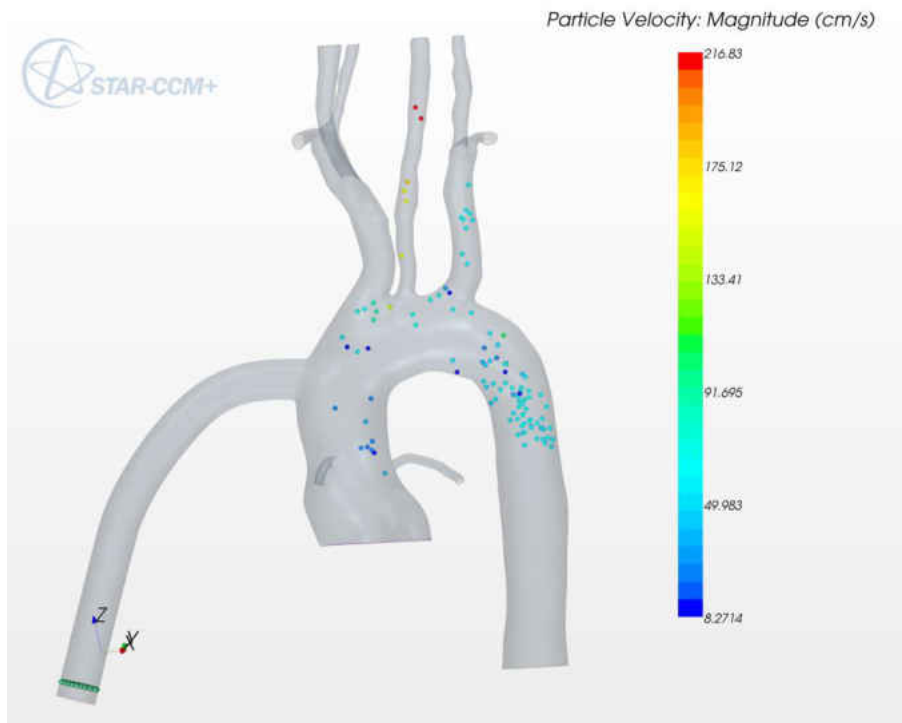
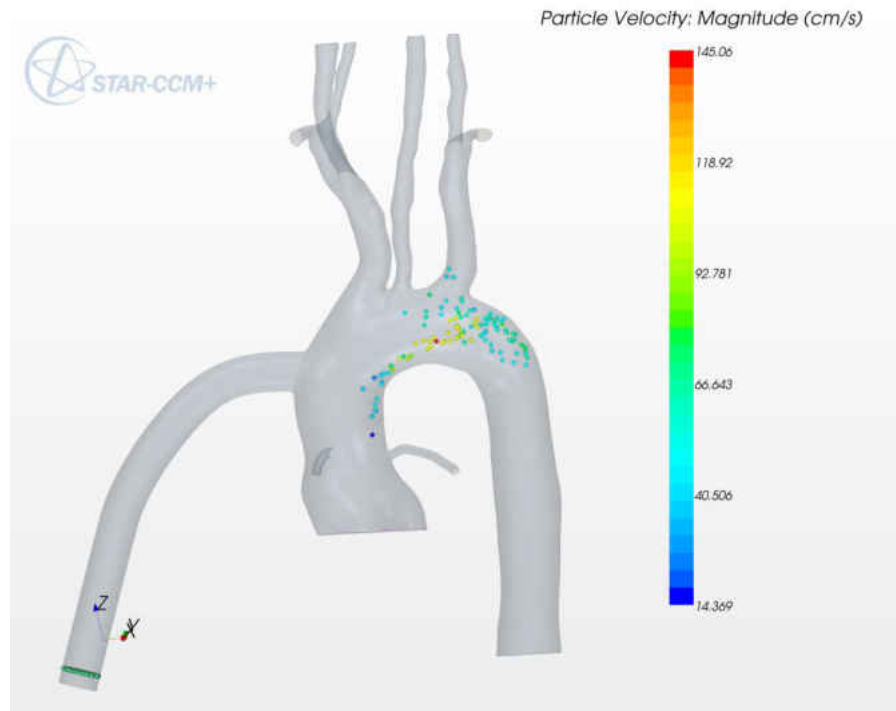


*Image taken from Starccm+ 8.02 visualization window*

*Figure 28 2mm motion distal to the LSA and descending aorta bifurcation for the 7-0 Model*

From the data observed it was also concluded that the number of cycles and its duration was also a big determinant on embolism probability. Particles that did not have enough momentum to reach an escape zone remained in the fluid domain until the maximum physical time was reached (0.75sec- one cycle). There were instances where particles were approaching or floating near an outlet but due to the time limit they never exited the system, thus not contributing towards the embolism statistic analysis. It is suggested to perform a new study in which there is more than one cycle.

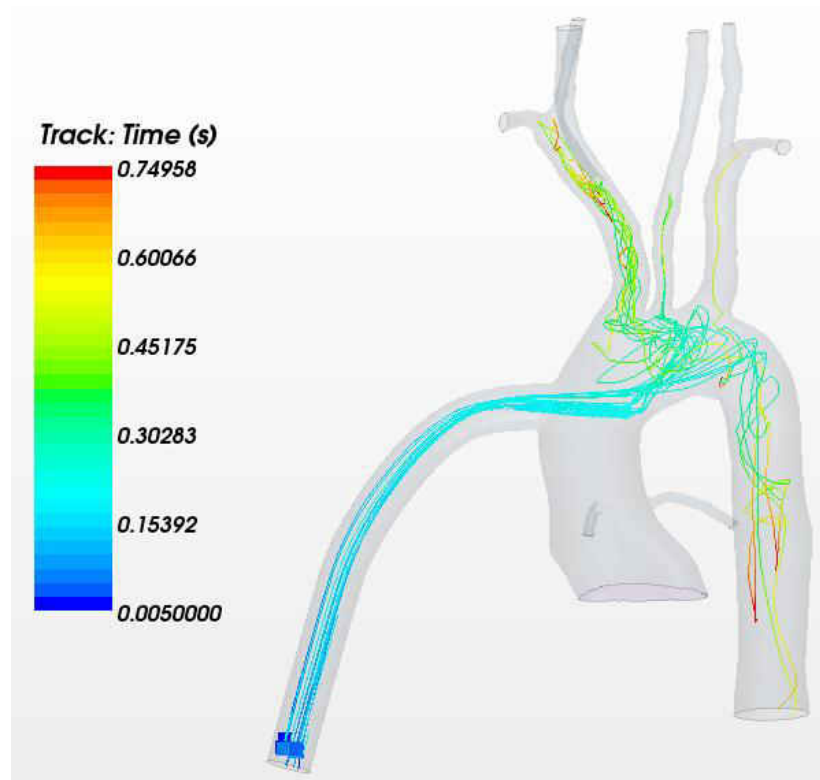


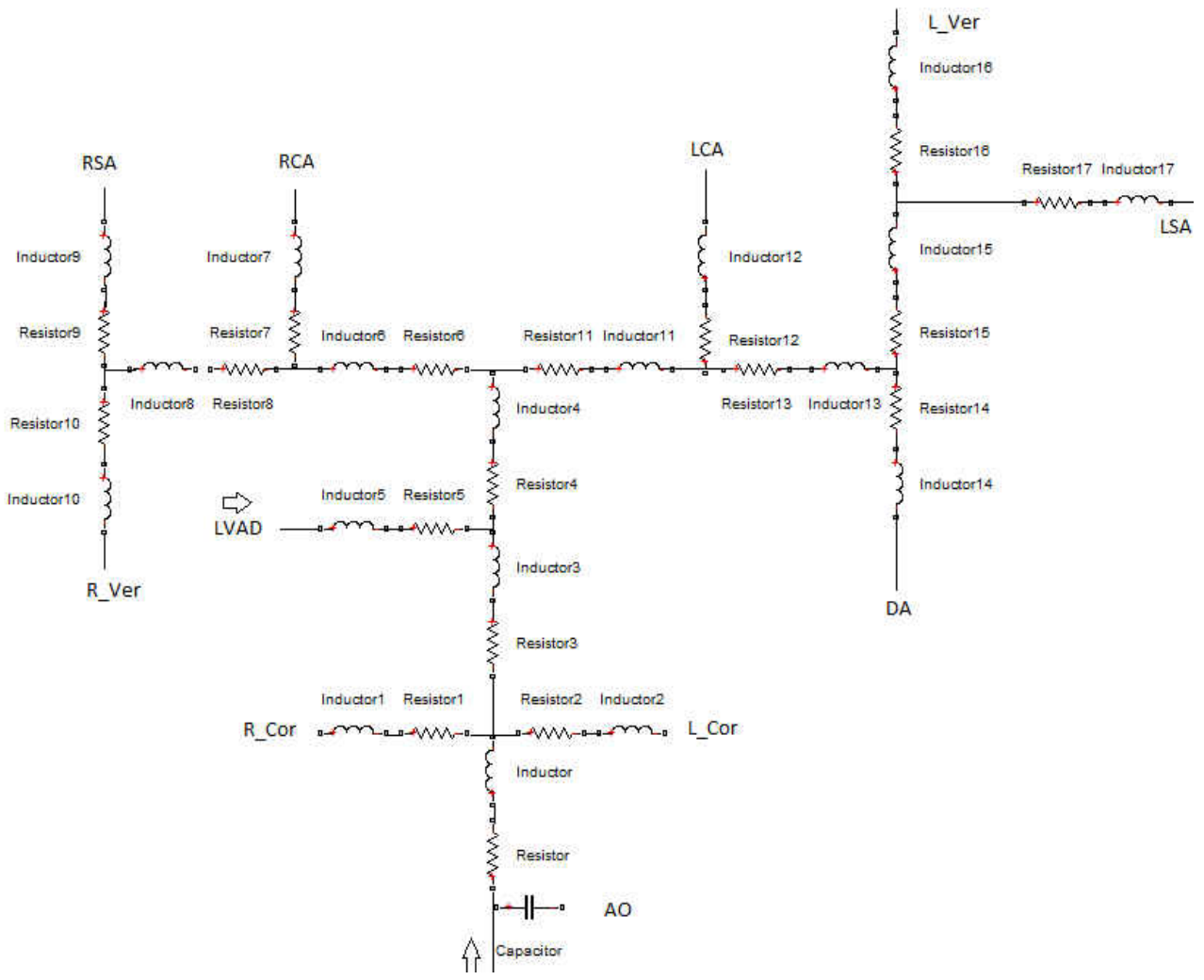
*Image taken from Starccm+ 8.02 visualization window*

*Figure 29 Tracks progression in time while in the fluid domain for 5mm*

Figure 29 shows the time spent by each 5mm particle for the 7-0 unsteady simulation. The hypothesis that 5mm particles were going to display a slower motion was confirmed, this occurs because the surface area in contact with the fluid is larger, then creating a larger drag force that will slow down the particle at a much faster rate when compared to a smaller diameter particle.

Overall we can conclude that unsteady flow does have an impact on the embolism probability. In the steady flow all the boundary conditions are continuously drawing flow at the same rate throughout the entire cycle, while the unsteady conditions at the outlets go from minimum extraction to a peak and then back down to the minimum. Particle motion is greatly affected by this phenomenon, because even though a particle can be near an outlet but it so happens that the cycle is going through the relaxation part of the cycle the particle will change direction as the flow slows down. In the future it will be interesting to see if statistics hold when allowing particles to reside for more than one cycle.

## APPENDIX: ONE DIMENSIONAL CIRCUIT SCHEMATIC





## LIST OF REFERENCES

- [I] B. Deswysen, A. C. (1980). Quantitative evaluation of the systemic arterial bed. *Medical and Biological Engineering and Computing* , 153-166.
- [II] Carol Lfavel, A., & Lynne Warner Stevenson, M. (2001). Take Hear with Heart Failure. *Circulation* , 89-91.
- [III] Ceballos, A. (2011). *A Multiscale Model of the Neonatal Circulatory System Following Hybrid Norwood Palliation*. Orlando.
- [IV] Chung, T. J. (2002). *Computational Fluid Dynamics*. Cambridge, UK: University Press.
- [V] George Faragallah, Y. W. (2012). A new control system for left ventricular assist devices based on patient specific physiological demand. *Inverse Problems in Science and Engineering* , 1-14.
- [VI] K.D. May-Newman, B. H. (2004). Effect of LVAD outflow conduit insertion angle on flow through the native aorta. *Medical Engineering & Technology* , 105-109.
- [VII] Li, J. K.-J. (2004). *Dynamics of the Vascular System*. Danvers: World Scientific Publishing Co.
- [VIII] N. Shahcheraghi, H. D. (2002). Unsteady and Three-Dimensional Simulation of Blood Flow in the Human Aortic Arch. *Transactions of the ASME* , 378-387.

- [IX] Oosterom, L. N. (2008). Left Ventricular Assist Device as a Bridge to Recovery in a Young Woman Admitted with Peripartum Cardiomyopathy. *Netherlands Heart Journal* , 426-428.
- [X] Osorio AF, O. R.-M. (2013). Computational fluid dynamics analysis of surgical adjustment of left ventricular assist device implantation to minimise stroke risk. *Computer Methods in Biomechanics and Biomedical Engineering* , 622-638.
- [XI] Suarez, J. C. (2011). Mechanisms of Bleeding and Approach to Patients With Axial Flow Left Ventricular Assist Devices. *Circulation* , 779-784.
- [XII] Taggart, S. a. (2008). *Biology: The Unity and Diversity of Life*. California: Wadsworth: Brooks Cole.
- [XIII] World Health Organization. (2013). Retrieved June 13, 2013, from World Health Organization: [http://www.who.int/cardiovascular\\_diseases/resources/atlas/en/](http://www.who.int/cardiovascular_diseases/resources/atlas/en/)
- [XIV] World Health Organization. (2001). *The Atlas of Heart Disease and Stroke*. Retrieved 06 12, 2013, from [http://www.who.int/cardiovascular\\_diseases/resources/atlas/en/](http://www.who.int/cardiovascular_diseases/resources/atlas/en/)